12

Multiobjective Optimal Design of an Inverter Fed Axial Flux Permanent Magnet In-Wheel Motor for Electric Vehicles

Christophe Versèle, Olivier Deblecker and Jacques Lobry
Electrical Engineering Department, University of Mons
Belgium

1. Introduction

Battery electric vehicles (EVs) and hybrid EVs are now at the forefront of transportation researches in order to reduce the emission of pollutant gasses, especially in the inner cities. However, the present performances of EVs are far from being competitive to those of traditional combustion engine vehicles, mainly in terms of autonomy. Therefore, power-saving and mass-saving are of the upmost importance when designing the entire drive system of EVs and their electric motor drives (Tseng & Chen, 1997).
In conventional EVs, the power system consists of battery, electric motors with drives, transmission gears and differentials to the wheels (Yang & Chuang, 2007). The mechanical transmission system contributes greatly to the power loss, through the heat dissipation in the various components, and to the weight of the vehicle. An interesting alternative to this conventional power system is the concept of in-wheel motors or hub-in motors as illustrated in Fig.1. In this concept, the motor is directly integrated into the wheel, thus eliminating transmission gears and differentials with their associated power loss (Yang et al., 2004). Furthermore, the elimination of mechanical components in transmission chains or gears reduces the weight of the vehicle. Each of the in-wheel motors has its own voltage supply inverter (VSI) as well as its own speed or torque controller. All the in-wheel motors are coordinated by a digital vehicular-speed controller with differential gear.
Due to their robustness, low cost, performances and simplicity of design, induction motors (IMs) are often preferred for EVs propulsion. However, in recent years, Neodymium-Iron-Bore (NdFeB) axial flux permanent magnet (AFPM) motors have become an interesting alternative to IMs due to their compactness, low weight and high torque density. Moreover, AFPM motors are pancake-type, fit perfectly the wheel of an automobile vehicle and, thus, can be easily and compactly integrated into the wheel. According to these properties, axial flux motors seem to be a better choice than more conventional radial flux motors for this kind of application. Note that this issue is discussed in (Versèle et al., 2009).
There are many alternatives for the design of AFPM motors (Sahin & Vandenput, 1999): slotted or slotless stator, rotor with interior or surface-mounted permanent magnets (PMs), internal or external rotor, numbers of rotors and stators, etc. In this chapter, a double-sided motor with internal slotted stator and surface-mounted PMs is proposed as basic design choice essentially motivated by the presence of two air gaps doubling the torque.

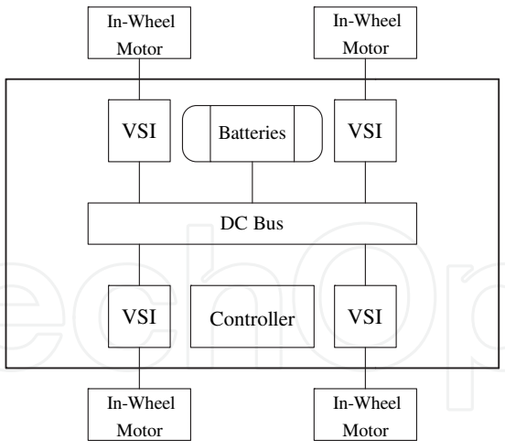

Fig. 1. In-wheel motors drive

Among the various researches, many authors have published papers about the optimal design of in-wheel motors for EVs or wheelchairs (Espanet et al., 1999; Nilssen et al., 2005; Tseng & Chen 1997; Yang et al., 2004) as well as about the optimization of AFPM motors (Azzouzi et al., 2006; Chun et al., 2007; Cvetkovski & Petkovska, 2002).
In this chapter, the objective is to optimize simultaneously one of the four in-wheel motors of an EV and its own VSI in terms of weight and power loss. Note that the simultaneous optimization of the in-wheel motor and its own VSI, rarely discussed in literature, results in a system optimized towards the requirements of the EV.
To do so, a multiobjective optimization (MO) technique based on evolutionary algorithms (EAs) is used. EAs are stochastic search techniques that mimic natural evolutionary principles to perform search and optimization procedure. Among the several approaches to evolutionary optimization, GAs have been chosen and the so-called Elitist Nondominated Sorting Genetic Algorithm (NSGA-II) (Deb, 2002) is used to perform the optimal design of the in-wheel motor and its own VSI. Note that GAs are chosen because they have already proved their efficiency to optimize every kind of electrical machines (Skaar & Nielssen, 2003) and power electronics converters (Helali, 2005; Malyna et al., 2007; Versèle et al., 2010).
The remainder of this chapter is organized as follows. First, the requirements in terms of power and torque of an EV are discussed in Section 2. Then, Section 3 describes the AFPM motor and VSI models used in the design procedure. In Section 4, the MO technique based on GAs as well as the proposed optimization routine are described. Finally, a design example is exposed in Section 5 and the advantages and limitations of the new design procedure are discussed in Section 6.

2. Requirements of an EV

In order to determine the requirements, in terms of power and torque, of one of the four in-wheel motors (considering an EV driven by four in-wheel motors), a computer model of an EV traction system is presented in this section.
The road load on the vehicle consists of three forces (Yang & Chuang, 2007): (1) the rolling resistance F_r, (2) the aerodynamic drag force F_a and (3) the climbing force F_c which are expressed as (Ehsani et al., 2005):

$$F_r = f_r M_v g \tag{1}$$

$$F_a = 0.5\rho A_f C_D \left(v + v_w\right)^2 \tag{2}$$

$$F_c = M_v g \sin\left(\alpha\right) \tag{3}$$

where f_r is the rolling resistance coefficient (which is an empirical coefficient depending on the road-tire friction), M_v is the mass of the vehicle, g is the earth gravity acceleration, ρ is the air density, A_f is the frontal area of the vehicle, C_D is the coefficient of aerodynamic resistance (that characterizes the shape of the vehicle), v is the vehicle speed, v_w is the component of the wind speed on the vehicle's moving direction and α is the road angle (deduced from the road slope). According to Newton's second law, the total tractive effort F_t required to reach the desired acceleration a and to overcome the road load is:

$$F_t = M_v a + F_r + F_a + F_c \,. \tag{4}$$

Once the total tractive effort is computed, the total torque T_t and power P_t required to be produced by the four in-wheel motors can be expressed as:

$$T_t = F_t r_{wheel} \tag{5}$$

$$P_t = T_t \Omega_{wheel} \tag{6}$$

where r_{wheel} is the drive wheels radius and Ω_{wheel} is the rotational wheels speed.
Based on the specifications of an urban EV (Ehsani et al., 2005), summarized in Table 1, and on the above-described EV traction system, the requirements of one in-wheel motor can be easily computed. All the results are presented in Table 2. Note that, in addition to provide its requirements, the in-wheel motor must also respect some constraints. The main constraints are the total weight of each of the four in-wheel motors M_{motor} (imposed by the maximal authorized "unsprung" wheel weight) and the imposed outer radius R_{out} of the motor (imposed by the rim of the wheel). Those are also specified in Table I and Table 2.

Weight M_v	1150 kg
Max. speed v_{max}	13.9 m/s (50 km/h)
Acceleration a	1 m/s²
Frontal area A_f	2.5 m²
Coefficient of aerodynamic resistance C_D	0.32
Rolling resistance coefficient f_r	0.015
Max. road angle a	5.7° (10%)
Rim diameter	14''
Number of in-wheel motors	4

Table 1. Specifications of an EV

Torque T_t	> 107 Nm
Power P_t	> 8.7 kW
Weight of the motor M_{motor}	< 43.125 kg

Table 2. Requirements of one in-wheel motor

3. Modeling of the AFPM motor and VSI

In order to evaluate the two objective functions, viz. the weight and the losses of the motor and the VSI, and to verify if the constraints are not violated during the design procedure, two models are necessary: one for the motor and one for the VSI. It should be noticed that analytical models have been chosen in this paper with the aim of reducing the computational time. These models permit to evaluate the weight and the losses of the motor and the VSI as well as to estimate the torque and power developed by the motor.

3.1 AFPM motor model

Analytical design of AFPM motors is usually performed on the average radius R_{ave} of the machine (Parviainen et al., 2003) defined by:

$$R_{ave} = \left(R_{in} + R_{out}\right)/2 \tag{7}$$

where R_{in} and R_{out} are respectively the inner and outer radius of the machine (see Fig. 2(a)).

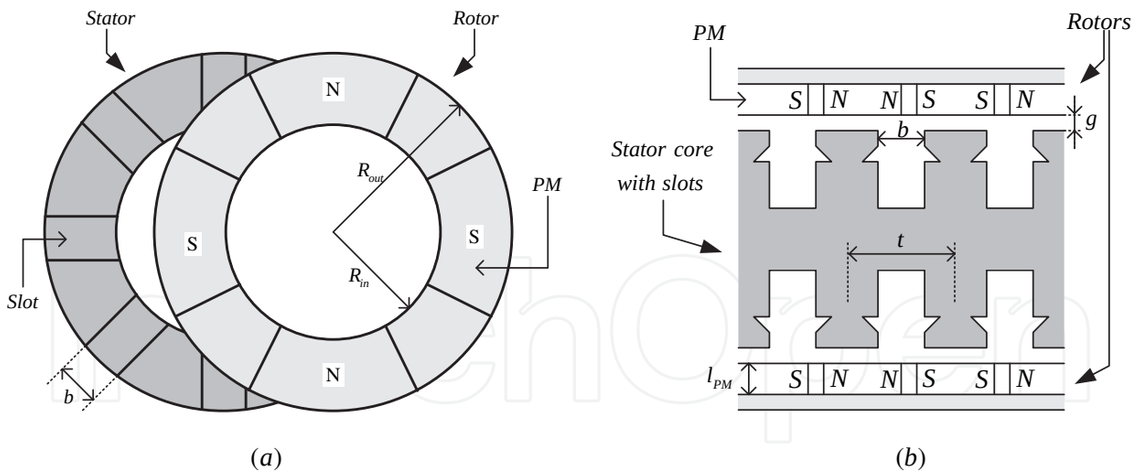

Fig. 2. (a) Stator and rotor of an AFPM machine and (b) doubled-sided AFPM machine with internal slotted stator

The use of the average radius as a design parameter allows evaluating motor parameters and performances based on analytical design methods (Gieras et al., 2004).
The air gap flux density B_g is calculated using the remanence flux density B_r (in the order of 1.2 T for a NdFeB type PM) and the relative permeability μ_{ra} of the PM as well as the geometrical dimensions of the air gap and the PM (thickness and area) according to:

$$B_g = k_{\sigma PM} \frac{B_r}{1 + \mu_{ra} \frac{k_C g}{l_{PM}} \frac{S_{PM}}{S_g}} \tag{8}$$

where g and l_{PM} are respectively the air gap thickness and PM thickness (see Fig. 2(b)); S_g and S_{PM} are respectively the air gap area and PM area. Finally, in (8), $k_{\sigma PM}$ (<1) is a factor that takes into account the leakage flux and k_C (>1) is the well-known Carter coefficient.

On the one hand, in order to obtain an accurate estimation of the air gap flux density and torque developed by the motor, the factor $k_{\sigma PM}$ is one of the most essential quantities that must be computed. Indeed, the leakage flux has a substantial effect on the flux density within the air gap and PMs (Qu & Lipo, 2002) and, therefore, on the torque developed by the motor (see (11)). In addition to air gap leakage flux, zigzag leakage flux is another main part of the leakage flux. The zigzag leakage flux is the sum of three portions (Qu & Lipo, 2002): the first part of the zigzag leakage flux is short-circuited by one stator tooth, the second part links only part of the windings of a phase and the third part travelling from tooth to tooth does not link any coil. Note that, in this paper, an analytical model developed by Qu and Lipo (Qu & Lipo, 2002) for the purpose of the design of surface-mounted PM machines is used to compute the factor $k_{\sigma PM}$. This model permits to express this factor in terms of the magnetic material properties and dimensions of the machine. It is thus very useful during the design stage.

On the other hand, the main magnetic flux density in the air gap decreases under each slot opening due to the increase in reluctance. The Carter coefficient permits to take into account this change in magnetic flux density caused by slot openings defining a fictitious air gap greater than the physical one. It can be computed as follows (Gieras et al., 2004):

$$k_C = \frac{t}{t - \gamma g} \tag{9}$$

where t is the average slot pitch (see Fig. 2(b)) and γ is defined by:

$$\gamma = \frac{4}{\pi}\left[\frac{b}{2g}\arctan\left(\frac{b}{2g}\right) - \ln\sqrt{1+\left(\frac{b}{2g}\right)^2}\right] \tag{10}$$

where b is the width of slot opening (see Fig. 2(b)).

Assuming sinusoidal waveform for the air gap flux density and the phase current, the average electromagnetic torque T of a double-sided AFPM motor can be calculated by:

$$T = 2\pi B_g A_{in} R_{out}^3 (k_d - k_d^3) \tag{11}$$

where A_{in} is the linear current density on the inner radius of the machine and k_d is the ratio between inner and outer radii of the rotor disk. It should be noticed that, for a given outer radius and magnetic and electric loading, the factor k_d is very important to determine the maximum torque developed by the motor. So, this factor will be one of the optimization variables. Figure 3 reports the per-unit (p.u.) electromagnetic torque with respect to this factor k_d. One can remark that the maximum value of the torque is reached for $k_d \approx 0.58$.

The electromagnetic power P can easily be calculated by the product of torque and rotational speed Ω_r of the motor according to:

$$P = T\Omega_r \,. \tag{12}$$

The double-sided AFPM motor losses are the sum of the stator winding losses, the stator and rotor cores losses, the PMs losses and the mechanical losses, whereas its weight is the sum of the stator and the two rotors weights, the stator winding weight and the PMs weight. Note that the computation of those different parts of the two objective functions can easily be found elsewhere (Gieras et al., 2004) and, so, it is not described in this chapter.
Finally, it should also be pointed out that some electrical parameters of the AFPM motor, such as the stator resistance (R_s) and the direct (L_d) and quadrature (L_q) axes inductances, can be calculated once the motor has been design using the above-described fundamental design equations.

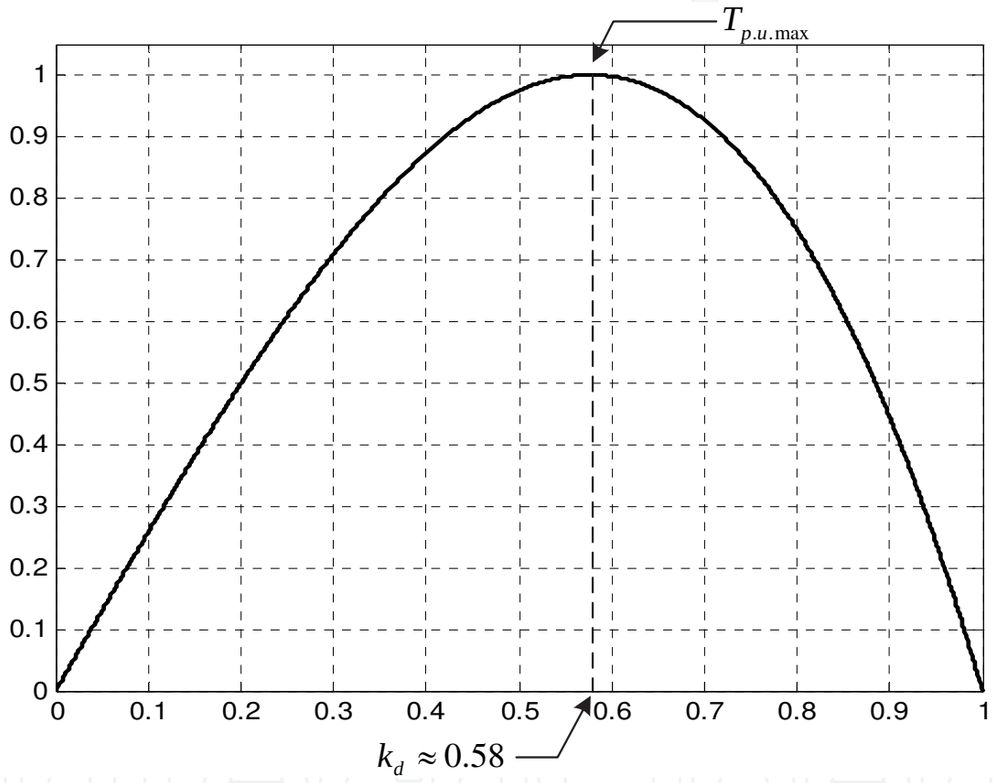

Fig. 3. Per-unit electromagnetic toque $T_{p.u}$ as a function of the factor k_d

3.2 AFPM motor model validation

In order to validate the analytical AFPM motor model presented in this chapter, analytical and experimental results are compared. To do so, the proposed model is applied to a 5.5 kW, 4000 rpm AFPM motor. The calculated motor parameters are then compared with parameters obtained by classical tests (test at dc level, no-load test, etc.) performed on an existing AFPM pump motor. All the results are reported in Table 3. As can be seen, very small differences are obtained between the analytical and experimental results, whatever the parameters. According to this validation method, one can conclude that the proposed analytical design process gives reasonable results in this particular case and can be used in the optimization procedure of the in-wheel motor of an EV.

Parameters	Analytical results	Experimental results
R_s (dc-resistance)	0.45 Ω	0.423 Ω
L_d	0,129 H	0,117 H
L_q	0,127 H	0,117 H
T	13.97 Nm	15.04 Nm
P	5.85 kW	5.5 kW

Table 3. Analytical and experimental results for the 5.5 kW, 4000 rpm AFPM pump motor

3.3 VSI model

The total loss of the semiconductor devices (IGBTs and diodes) of the VSI (employing sinusoidal pulse-width-modulation) consists of two parts: the on-state losses and the switching losses. The on-state losses of the devices are calculated from their average I_{ave} and rms I_{rms} currents by the well-known expression (Semikron, 2010):

$$P_{on} = V_{th} \cdot I_{ave} + r \cdot I_{rms}^2 \tag{13}$$

where V_{th} represents the threshold voltage and r the on-state resistance, both taken from the manufacturer's data sheets.

The switching losses are, as for them, calculated by the following formula (Semikron, 2010):

$$P_{sw} = f_s \cdot \left(E_{turn-on} + E_{turn-off} \right)_{T_j, I_C, V_{CE}} \tag{14}$$

where $E_{turn\text{-on}}$ and $E_{turn\text{-off}}$ are the energies dissipated during the transitions, both taken from the manufacturer's data sheets, at given junction temperature T_j, on-state collector current I_C and blocking voltage V_{CE}. Note that the average and rms values of the current used in (13) can easily be computed.

Based on the total loss of the semiconductor devices, the heatsink can be designed in order to limit the junction temperature to a predefined temperature (typically in the order of 125 °C). This temperature can be estimated from the ambient temperature T_a, the thermal resistances (junction-case: $R_{th,jc}$, case-heatsink: $R_{th,ch}$ and heatsink-ambient: $R_{th,ha}$) and the total loss P_{sc} of all the semiconductor devices by:

$$T_j = T_a + \left(R_{th,jc} + R_{th,ch} + R_{th,ha} \right) \cdot P_{sc} \,. \tag{15}$$

From (15), the thermal resistance of the heatsink $R_{th,ha}$ needed to limit the junction temperature to the predefined value can be computed and, then, the heatsink can be selected from the manufacturer's data sheets.

The total weight of the VSI is the sum of the weight of all the semiconductor devices and the weight of the heatsink.

4. Optimization routine based on the NSGA-II

As mentioned previously, in this contribution, a MO technique based on EAs is used. Those are stochastic search techniques that mimic natural evolutionary principles to perform the search and optimization procedures (Deb, 2002).

GAs have been chosen because they overcome the traditional search and optimization methods (such as gradient-based methods) in solving engineering design optimization problems (Deb & Goyal, 1997). Indeed, there are, at least, two difficulties in using traditional optimization algorithms to solve such problems. Firstly, each traditional optimization algorithm is specialized to solve a particular type of problems and, therefore, may not be suited to a different type. As this is not the case with the GAs, no particular difficulties have been met to adapt the considered GA (viz. the NSGA-II, see below) to the multiobjective optimal design of the AFPM motor and its VSI. Only the models of these converters had to be used in combination with the GA in order to evaluate the values of the considered objectives. Secondly, most of the traditional methods are designed to work only on continuous variables. However in engineering designs, some variables are restricted to take discrete values only. In this chapter, this requirement arises, e.g., for the choice of the number of poles pairs.

Mixed-variable optimization problems are difficult to tackle because they pose the problems of the combinatorial and continuous optimization problems (Socha, 2008). For this reason, there are not many dedicated algorithms in literature and most of the approaches used in these algorithms relax the constraints of the problem. The most popular approach consists in relaxing the requirements for the discrete variables which are assumed to be continuous during the optimization process (Deb & Goyal, 1997). This type of approach is, often, referred as continuous relaxation approach.

Apart from the relaxation-based approach, there are methods proposed in literature that are able to natively handle mixed-variable optimization problems. However, only a few such methods have been proposed. Among them, the Genetic Adaptive Search is based on the fact that there are versions of the GAs dedicated to discrete variables and other versions dedicated to continuous variables. So, the GAs can be easily extended to natively handling both continuous and discrete variables. Such an approach has been proposed in (Deb & Goyal, 1997) and will be used in this chapter as it has already proved to be efficient to solve engineering problems (see, e.g. (Deb & Goyal, 1997)). Pattern Search Method (Audet & Dennis, 2001), Mixed Bayesian Optimization Algorithms (Ocenasek & Schwarz, 2002) and Ant Colony optimization (Socha, 2008) are other methods which permit to tackle mixed-variable problems.

Among the several MO techniques using GAs (see, e.g., (Deb, 2007)), the so-called NSGA-II (Deb *et al.*, 2002), described in the next Section, will be used to perform the optimal design.

4.1 NSGA-II

NSGA-II is a recent and efficient multiobjective EA using an elitist approach (Deb, 2002). It relies on two main notions: nondominated ranking and crowding distance. Nondominated ranking is a way to sort individuals in nondominated fronts whereas crowding distance is a parameter that permits to preserve diversity among solutions of the same nondominated front. The procedure of the NSGA-II is shown in Fig. 4 and is as follows (Deb, 2002). First, a combined population R_t (of size $2 \cdot N$) of the parent P_t and offsprings Q_t populations (each of size N) is formed. Then, the population R_t is sorted in nondominated fronts. Now, the solutions belonging to the best nondominated set, i.e. F_1, are of best solutions in the combined population and must be emphasized more than any other solution. If the size of F_1 is smaller than N, all members of F_1 are inserted in the new population P_{t+1}. Then, the remaining population of P_{t+1} is chosen from subsequent nondominated fronts in order of

their ranking. Thus, the solutions of F_2 are chosen next, followed by solutions from F_3. However, as shown in Fig. 4, not all the solutions from F_3 can be inserted in population P_{t+1}. Indeed, the number of empty slots of P_{t+1} is smaller than the number of solutions belonging to F_3. In order to choose which ones will be selected, these solutions are sorted according to their crowding distance (in descending order) and, then, the number of best of them needed to fill the empty slots of P_{t+1} are inserted in this new population. The created population P_{t+1} is then used for selection, crossover and mutation (see below) to create a new population Q_{t+1}, and so on for the next generations.

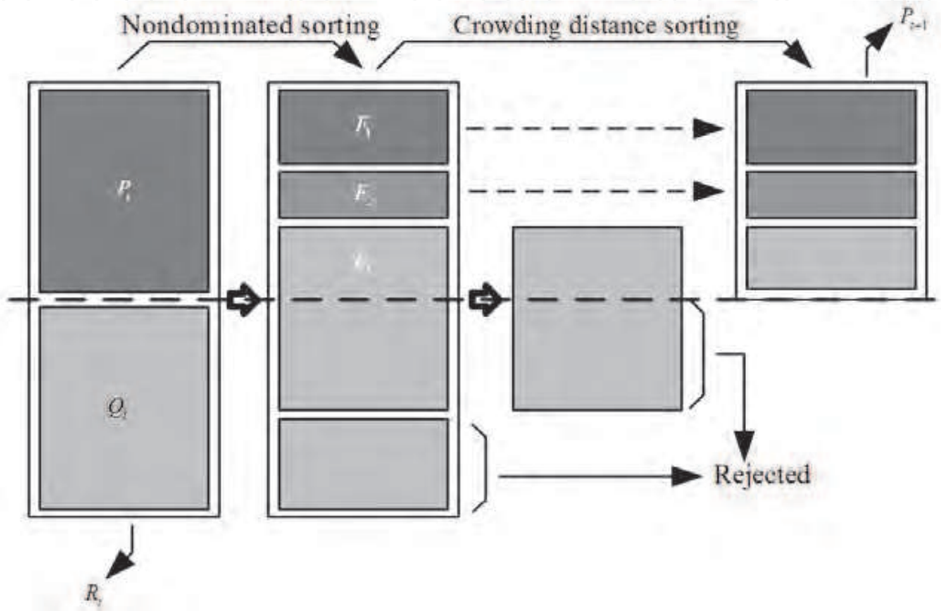

Fig. 4. NSGA-II procedure (Deb, 2002)

NSGA-II has been implemented in Matlab with real and binary coding schemes. So, a discrete variable is coded in a binary string whereas a continuous variable is coded directly. Such coding schemes are used in this paper because the considered optimization variables (see Table 4 in Section 5) belong to the two categories.

These coding schemes allow a natural way to code different optimization variables, which is not possible with traditional optimization methods. Moreover, the real coded scheme for the continuous variables eliminates the difficulties (Hamming cliff problem and difficulty to achieve arbitrary precision) of coding such variables with a binary scheme.

So, e.g., with the coding scheme used in this paper, the structure of the chromosome (composed by the seven considered optimization variables) of the solution #3 (see Table 5 in Section 5) is as follows:

$$\underbrace{(k_d)(J)(l_{PM})(g)(f_s)}_{\text{real coded variables}}\quad\underbrace{(p)(q)}_{\text{binary coded variables}}$$

$$\downarrow$$

$$(0.89)(4.9)(5)(1.9)(1972)\underbrace{(1110)}_{\rightarrow 14}\underbrace{(11011110)}_{\rightarrow 222}$$

There are three fundamental operations used in GAs: selection, crossover and mutation. The primary objective of the selection operator is to make duplicate of good solutions and eliminate bad solutions in a population, in keeping the population size constant. To do so, a tournament selection (Deb, 2002) based on nondominated rank and crowding distance of each individual is used. Then, the selected individuals generate offsprings from crossover and mutation operators. To cross and to mutate the real coded variables the Simulated Binary Crossover and Polynomial Mutation operators (Deb & Goyal, 1997) are used in this chapter. The single-point crossover (Deb, 2002) is, as for it, used to cross the discrete optimization variables. Note that to mutate this type of variables, a random bit of their string is simply changed from '1' to '0' or *vice versa*.
Finally, the constraints must be taken into account. Several ways exist to handle constraints in EAs. The easiest way to take them into account in NSGA-II is to replace the non-dominated ranking procedure by a constrained non-dominated ranking procedure as suggested by its authors elsewhere (see, e.g., (Deb, 2002)). The effect of using this constrained-domination principle is that any feasible solution has a better nondominated rank than any infeasible solution.
It is important to emphasize that the GA must be properly configured. The size of the population is one of the important parameters of the GA as well as the termination criterion. In this contribution, the size of the population N is taken equal to 100. It is important to note that, on the one hand, N should be large enough to find out small details of the Pareto front whereas, on the other hand, N should not be too large to avoid long time optimization. The termination criterion consists in a pre-defined number of generations which is here also fixed to 400. Finally, the crossover probability and the mutation probability are respectively chosen to be 0.85 and 0.015 as typically suggested in literature (Deb, 2002).

4.2 Design procedure

The overall design procedure, presented in Fig. 5, has been implemented in the Matlab environment. First, a random initial population is generated. Then, the objective functions, i.e. the total weight and the total losses of the VSI-fed AFPM in-wheel motor, are evaluated based on the initial population and on the above-described models (see Section 3). A convergence test is then performed to check for a termination criterion. If this criterion is not satisfied, the reproduction process using genetic operations starts. A new population is generated and the previous steps are repeated until the termination criterion is satisfied. Otherwise, the Pareto front, i.e. the nondominated solutions within the entire search space, is plotted and the optimization procedure ends.

5. Design example

In order to illustrate the design procedure, a VSI-fed AFPM in-wheel motor with the specifications given in Tables 1 and 2 is designed in this Section.
The lower and upper bounds of the seven considered optimization variables, viz. the factor k_d, the current density in the conductors J, the air gap thickness g, the PMs thickness l_{PM}, the number of poles pairs p, the number of slots q and the switching frequency f_s, are specified in Table 4. Note that the variables p and q are discrete ones whereas the others are continuous.
It should also be recalled that the in-wheel motor must provide the requirements of the EV as well as respect some constraints. The main constraints are the total weight M_{motor} of each of the four in-wheel motor and the imposed outer radius of the motor R_{out}. Note that these constraints have already been specified in Tables 1 and 2.

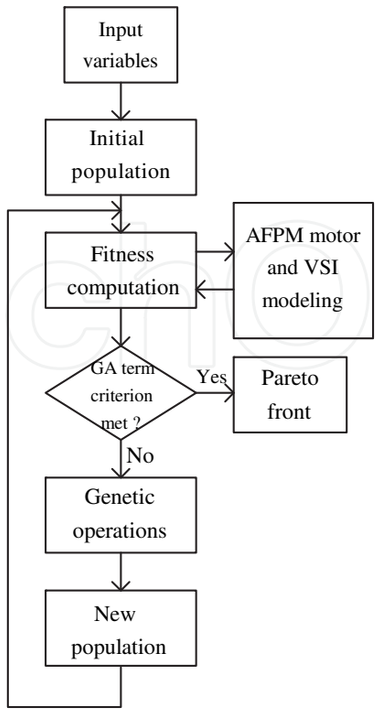

Fig. 5. Flowchart of the design procedure using GAs

Variables	Bounds	Type
k_d	[0.5 ; 0.9]	Continuous
J	[1 ; 6] A/mm²	Continuous
l_{PM}	[1 ; 20] mm	Continuous
g	[1 ; 5] mm	Continuous
f_s	[1 ; 10] kHz	Continuous
p	[1 ; 15]	Discrete
q	[50 ; 255]	Discrete

Table 4. Optimization variables

The results, i.e. the Pareto front, are presented in Fig. 6. Each point of this Pareto front represents an optimal VSI-fed AFPM in-wheel motor that respects all the constraints. Moreover, the values of the optimization variables corresponding to three particular solutions of the front are detailed in Table 5.

For a practical design, one particular solution of the Pareto front should be chosen. On the one hand, the choice of this particular solution can be let to the designer who can choose *a posteriori* which solution best fits the under consideration application or which objective function to promote. Moreover, in industrial framework, this set of solutions can be confronted with additional criteria or engineer's know-how not included in models.

On the other hand, the designer can also use some dedicated techniques to choose a particular solution of the Pareto front. These can be categorized into two types (Deb, 2002): post-optimal techniques and optimization-level techniques.

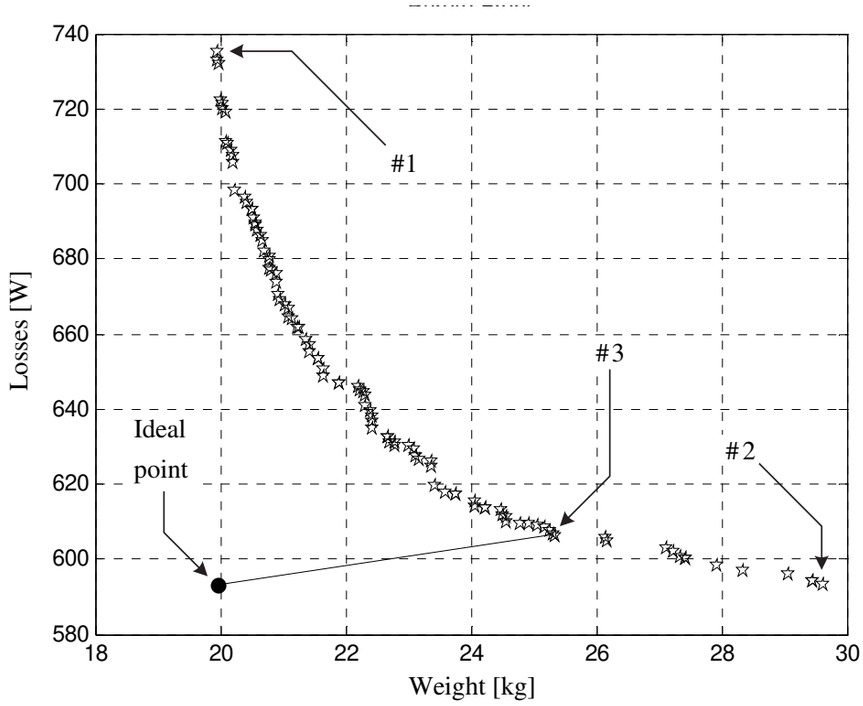

Fig. 6. Pareto front

	#1	#2	#3
k_d	0.89	0.89	0.88
J [A/mm²]	4.9	5.5	4.9
l_{PM} [mm]	5	5	5
g [mm]	1.9	3.2	1
f_s [Hz]	1972	2110	1410
p	14	15	10
q	222	255	158
T_t [Nm]	207	208	207
P_t [kW]	8.72	8.77	8.72
M_{Motor} [kg]	17.2	15.1	26

Table 5. Details of three particular solutions

In the first approach, the solutions obtained from the optimization technique are analyzed to choose a particular solution whereas, in the second approach, the optimization technique is directed towards a preferred region of the Pareto front. Therefore, only the techniques belonging to the first category are helpful in this chapter. Among these techniques, the Compromise Programming Approach (CPA) (Yu, 1973) is often used in multiobjective problems. The CPA picks a solution which is minimally located from a given reference point (e.g. the ideal point which is a nonexistent solution composed with the minimum value of the two objectives). Note that other techniques, such as the Marginal Rate of Substitution Approach (Miettinen, 1999), the Pseudo-Weight Vector Approach (Deb, 2002) or a method based on a sensitivity analysis (Avila *et al.*, 2006), can also be used.

For instance, using the CPA, the solution #3 of the Pareto front is minimally located from the ideal point. This solution can therefore be considered for a practical design and corresponds, moreover, to a good trade-off between the two objectives.
The evolution of the percentage of individuals belonging to the first nondominated front during the optimization procedure is shown in Fig. 7. From this figure, one can easily conclude that all the individuals are located in the first front at the end of this procedure. Moreover, it can also be observed that new nondominated solutions have been found after approximately 150 generations.
From Fig. 8, it can be conclude that all the individuals respect all the constraints since the fourth generation.
In order to study more in details the evolution of the optimization variables, their values have been plotted along the Pareto front (as a function of the weight) in Fig. 9 to Fig. 15. From these figures, it can be concluded that some of them have converged to an optimal value.

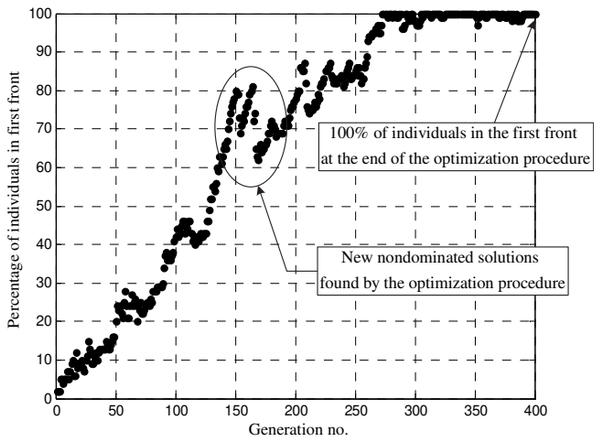

Fig. 7. Evolution of the percentage of individuals belonging to the first nondominated front during the optimization procedure

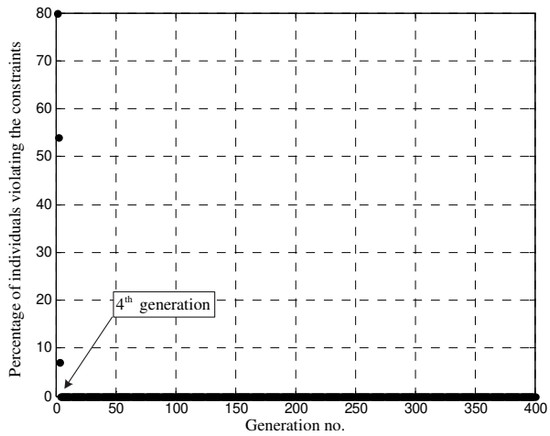

Fig. 8. Evolution of the percentage of individuals violating the constraints during the optimization procedure

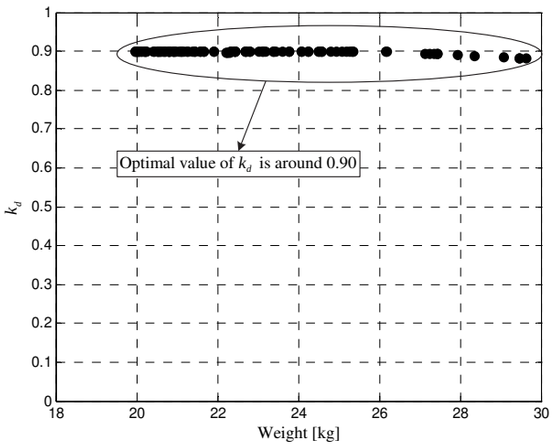

Fig. 9. Evolution of k_d along the Pareto front

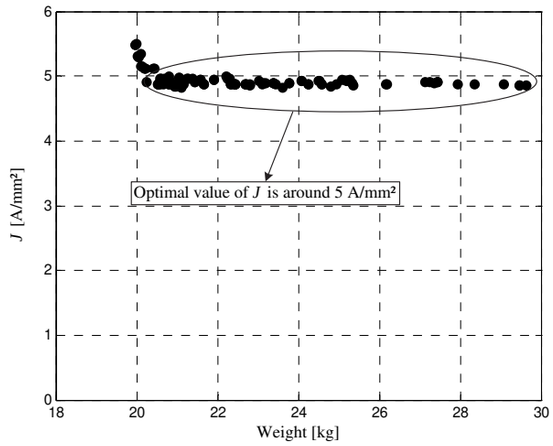

Fig. 10. Evolution of J along the Pareto front

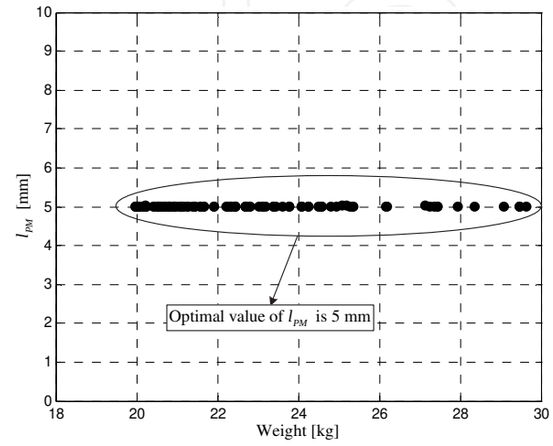

Fig. 11. Evolution of l_{PM} along the Pareto front

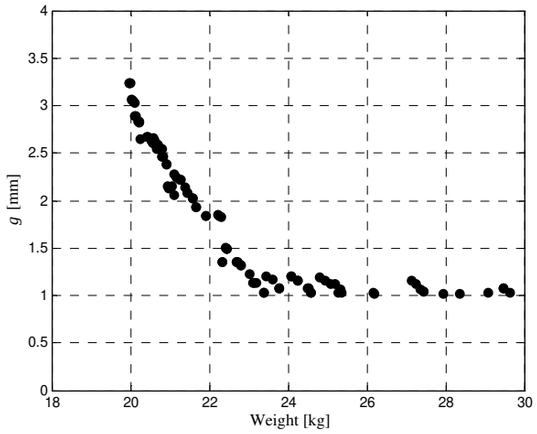

Fig. 12. Evolution of g along the Pareto front

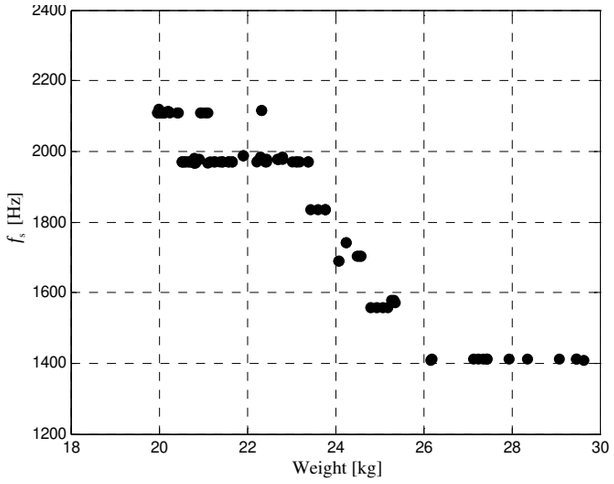

Fig. 13. Evolution of f_s along the Pareto front

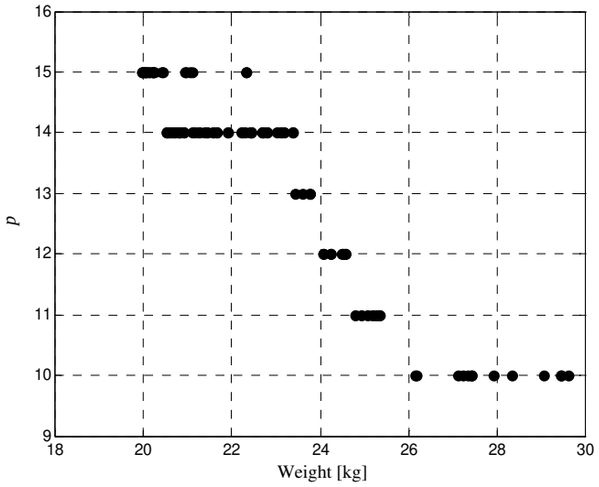

Fig. 14. Evolution of p along the Pareto front

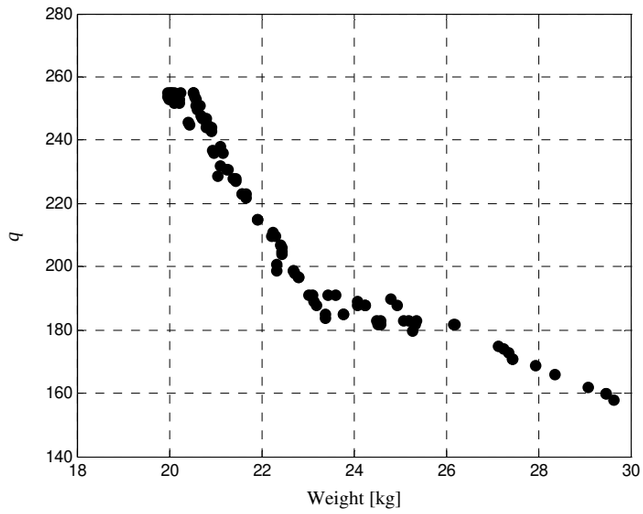

Fig. 15. Evolution of q along the Pareto front

First, the optimal value of the factor k_d is around 0.90 (see Fig. 9). Based on the Fig. 3, one can expect that this value would have converged to 0.58. However, this result is not surprising. Indeed, it has been show elsewhere (Azzouzi et al., 2006) that the maximum value of the torque to weight ratio is obtained for values of k_d around 0.85 and, in this chapter, the weight must be minimized.

Second, the optimal value of J is around 5 A/mm² as shown in Fig. 10 and, third, l_{PM} has converged to the optimal value of 5 mm (see Fig. 11).

In order to further analyze the optimization results, a study of the correlation level between the optimization variables and the objective functions is performed. The results are graphically represented in Fig. 16 and discussed below. Note that a positive value of the correlation factor indicates that the objective function grows when the optimization variable grows whereas a negative value indicates that the objective function reduces when the optimization variable grows.

From Fig. 16, it can be concluded that the optimization variables which have not converged to an optimal value, viz. g, f_s, p and q, have a significant influence on the two objective functions. Indeed, the correlation coefficient between each variable and each objective are, in absolute value, equal or greater than 0.8. The correlations are therefore strong. The fact that the correlation factors between k_d or J and the objective value are smaller is due to the fact that these variables have converged around an optimal value. Moreover, the fact that l_{PM} has converged to an optimal value leads to a correlation coefficient close to zero.

One can easily conclude that the variables p and f_s have the bigger influence on the weight (correlation coefficients equal to -0.94) whereas the variable g has the greater influence on the power loss (correlation coefficient equal to 0.98). Figure 16 also justifies the use of a MO technique. Indeed, the two objective functions are conflicting with respect to the optimization variables (except for l_{PM}) since the correlation levels are of opposite signs.

Finally, the distribution of the weight and the power loss among the AFPM motor and the VSI for the three particular solutions presented in Table 5 are respectively shown in Fig. 17 and Fig. 18 respectively. Figures 19 and 20 present, as for them, the distribution of these two objectives among the several parts of the motor (stator, rotor, PMs and windings).

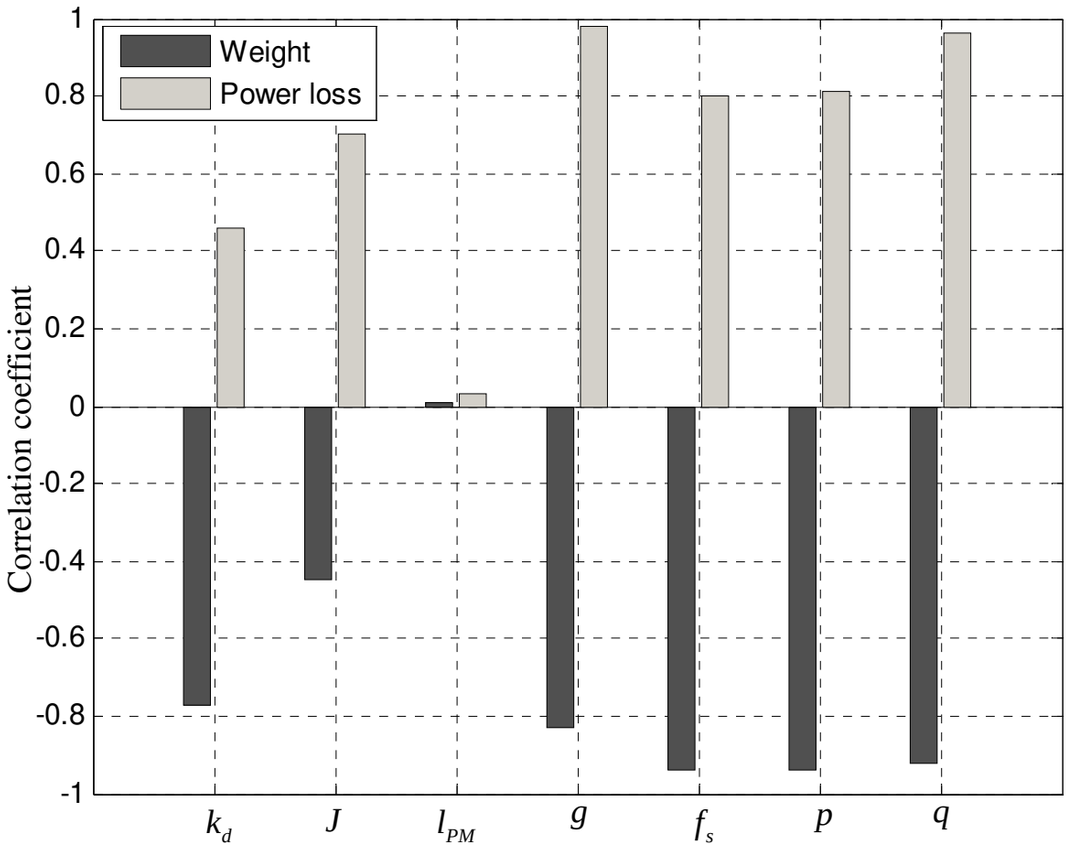

Fig. 16. Correlation between the optimization variables and the objective functions

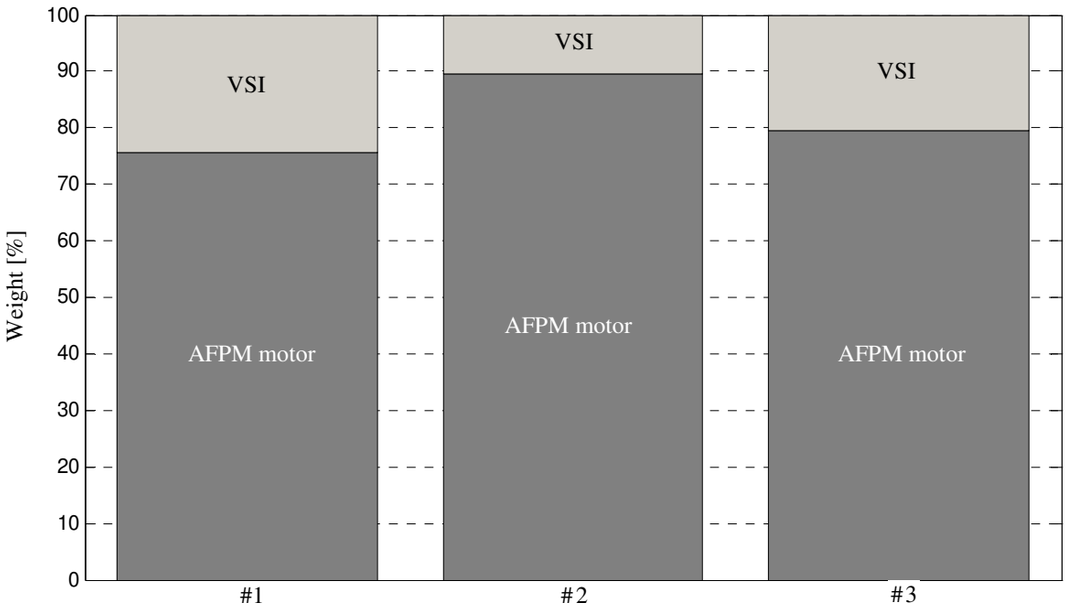

Fig. 17. Distribution of the weight among the AFPM motor and the VSI

Figure 17 shows that the major contributor in weight is the AFPM motor. Indeed, it represents at least 75% of the total weight. Instead, the power loss is, as for it, more equally distributed among the two parts. In fact, approximately 60% of the loss is due to the motor (see Fig. 18).
Figure 19 shows that the PMs are the minor contributor in terms of weight and represent more or less 5% to 10% of the total weight whatever the solution. One can also conclude that the rotor is the heavy part of the AFPM motor.

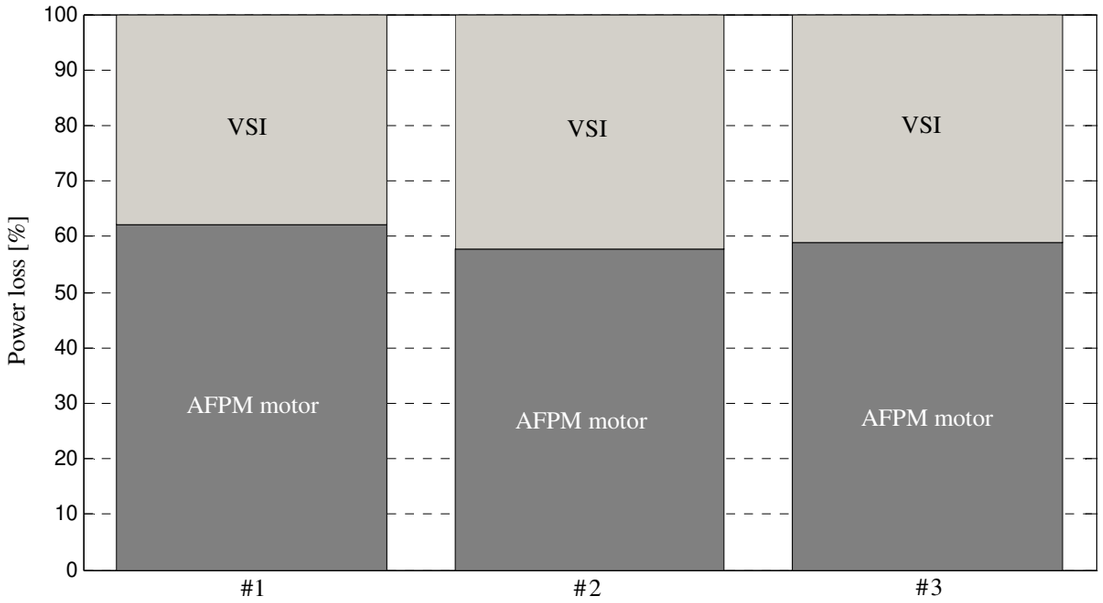

Fig. 18. Distribution of the power loss among the AFPM motor and the VSI

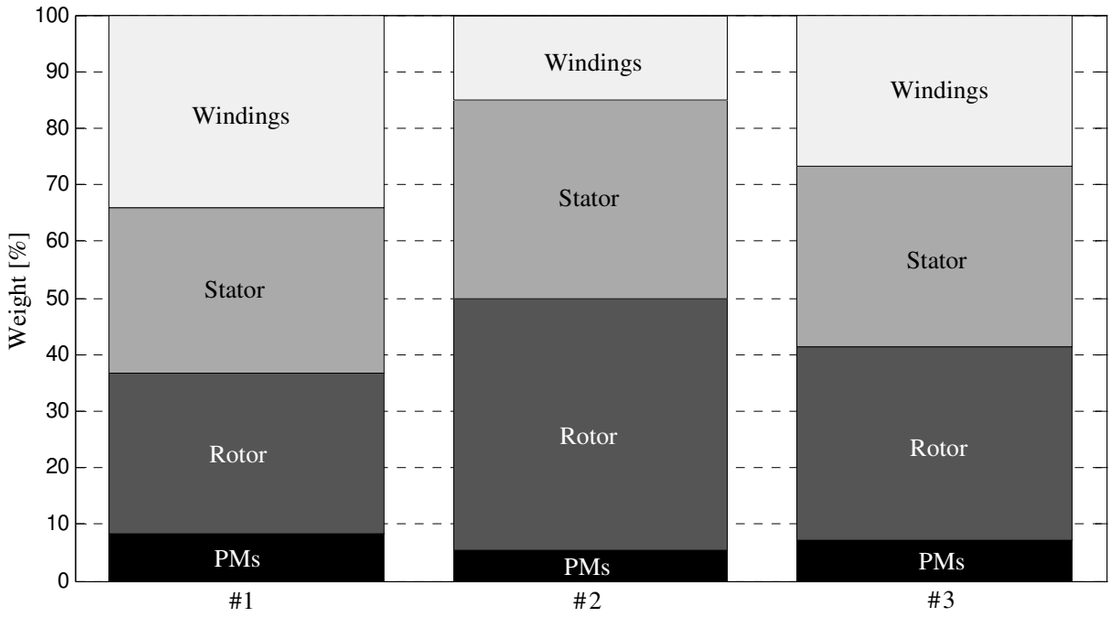

Fig. 19. Distribution of the weight among the several parts of the AFPM motor

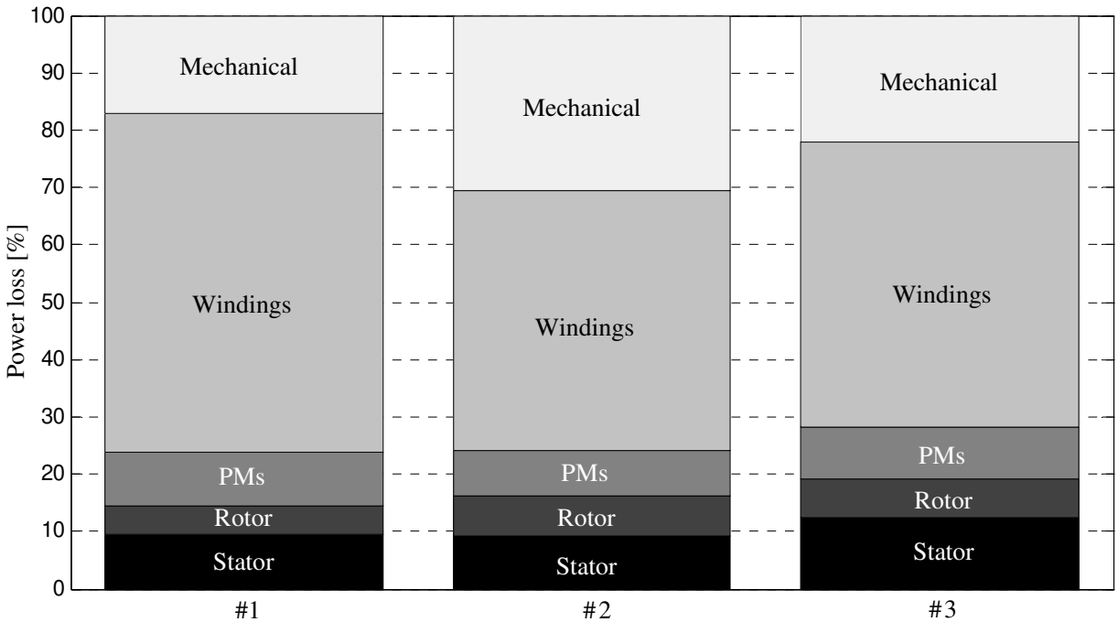

Fig. 20. Distribution of the power loss among the several parts of the AFPM motor

In solution #2, the stator and rotor weights largely dominate the winding and PMs weights compared with the other solutions. This can be explained regarding the value of the flux density in the air gap. Indeed, this value is the greatest among the three solutions (in the order of 0.90 T). So, the stator and rotor must be thick enough to avoid saturation of steel. As these thicknesses are computed using the air gap flux density, the stator and rotor of the solution #2 are thicker and, therefore, heavier. Moreover, the windings of the solution #2 are lighter than the windings of the two other solutions since the frequency is greater. Indeed, according to Faraday's law (Mohan et al., 2003), the windings turns necessary to obtain a same electromotive force is less than in the other solutions which, therefore, yields lighter windings realization.
As can be easily seen from Fig. 20, the mechanical and, more especially, the winding losses are the major contributors in terms of power loss. The fact that the winding losses are so high can be explained by the medium frequency effects (skin and proximity effects).

6. Advantages and limitations of the design procedure

The design procedure proposed in this paper presents several advantages but also some limitations.
A first advantage of this design procedure is that it is multiobjective. So, several conflicting objectives, often present in engineering design problems, can be optimized simultaneously.
A second advantage is the number of solutions considered in a small time. Indeed, the optimization procedure compares a large number of solutions (in the order of several thousands) to retain only the best in a time of approximately 120 s (for 400 generations of 100 individuals with a Pentium (R) D CPU 3.40 GHz, 3 Go RAM).
A third advantage is the simultaneous optimization of the in-wheel motor and its own VSI. Indeed, it results in a system optimized towards the requirements of the EV.

At last, the design procedure has the major advantage that a set of optimal solutions – instead of a single one – is proposed to the designer who can choose *a posteriori* which objective function to promote and, then, select a particular VSI-fed in-wheel motor. So, a degree of freedom is still available at the end of the optimization procedure. Moreover, in industrial framework, this set of solutions can be confronted with additional criteria or engineer's know-how not included in models.

The main limitation of the design procedure is related to the analytical modeling of the AFPM motor. Indeed, an analytical modeling of such motor can lead to a lack of accuracy in some cases, e.g. with a PM shape of higher complexity when the magnet occupation ratio varies along the radius of the rotor (Parviaien et al., 2003). This lack of accuracy arises from the reduction of the 3D design problem to a 2D design problem performed on the average radius of the machine.

It should also be noticed that the most accurate method to predict the performances of an AFPM motor is a 3D finite element analysis (FEA) but it is often too much time consuming to be included in an optimal design procedure in which a large numbers of solutions have to be evaluated. Therefore, the optimal design procedure presented in this contribution is very useful during the first stages of the design, although more sophisticated methods, such as 2D or 3D FEA, are required in more advanced phases of the design.

Note that, in this chapter, the magnet occupation ratio has been considered as constant along the radius of the rotor and, therefore, this limitation is not taken into account in the design of the AFPM motor.

7. Conclusion

This chapter has addressed the problem of MO design of a VSI-fed AFPM synchronous motor using GAs and a new design procedure has been proposed. The weight and the losses of both the motor and the VSI have been chosen as objective functions whereas the factor k_d, the current density in the conductors, the air gap thickness, the PMs thickness, the number of poles pairs, the number of slots and the switching frequency have been chosen as optimization variables. Finally, the design procedure has been illustrated by the design of a VSI-fed AFPM in-wheel motor for an urban EV and some conclusions have been drawn.

Finally, recall that, although many authors have published papers about the optimal design of in-wheel motors for EVs, the simultaneous optimization of the in-wheel motor and its own VSI has, to the authors' knowledge, rarely been discussed in literature.

8. References

Audet, C. & Dennis Jr., J. (2001). Pattern search algorithms for mixed variable programming. *SIAM Journal on Optimization*, vol. 11, no. 3, (July 2001), pp. 573-594, ISSN 1052-7189.

Avila, S. L.; Lisboa, A. C.; Krähenbühl L.; Carpes, Jr. W. P.; Vasconcelos, J. A.; Saldanha, R. R.; & Takahashi, R. H. C. (2006). Sensitivity Analysis Applied to Decision Making in Multiobjective Evolutionary Optimization, *IEEE Transactions on Magnetics*, vol. 42, no. 4, (April 2006) , pp. 1103-1106, ISSN 0018-9464.

Azzouzi, J.; Belfkira, R..; Abdel-Karim, N.; Barakat G. & Dakyo, B. (2006). Design Optimization of an Axial Flux PM Synchronous Machine: Comparison Between DIRECT Method and GAs Method, *Proceedings of 12th International Power Electronics*

and Motion Control Conference, ISBN 1-4244-0121-6, Portoroz, Slovenia, September 2006.

Chun, Y. D.; Koo, D.-H. & Cho, Y.-H. (2007). Multiobjective optimization design of axial flux permanent magnet motor. *International Journal of Applied Electromagnetics and Mechanics*, vol. 25, no. 1, (January 2007), pp. 613-619, ISSN 8273-284.

Cvetkovski, G. & Petkovska, L. (2008). Efficiency Maximisation in Structural Design Optimisation of Permanent Magnet Synchronous Motor, *Proceedings of 18th International Conference on Electrical Machines*, ISBN 978-1-4244-1736-0, Vilamoura, Portugal, September 2008.

Deb, K. & Goyal, M. (1997). Optimization Engineering Designs Using a Combined Search, *Proceedings of 7th International Conference on Genetic Algorithms*, ISBN 1-55860-299-2, East Lansing, USA, July 1997.

Deb, K. (2002). *Multi-Objective Optimization using Evolutionary Algorithms*, John Wiley & Sons, Inc., ISBN 0470743611, New Jersey, USA.

Deb, K. (2007). Current trends in evolutionary multi-objective optimization, *International Journal for Simulation and Multidisciplinary Design Optimization*, vol. 1, no. 1, (December 2007), pp. 1-8., ISSN 1779-6288.

Ehsani, M.; Gao, Y.; Gay, S. E. & Emadi, A. (2006). *Modern Electric, Hybrid Electric and Fuel Cell Vehicles: Fundamentals, Theory, and Design*, CRC Press, ISBN 0-8493-3154-4, Florida, USA.

Espanet, C.; Kauffmann, J. M.; Wurtz, F. & Bigeon, J. (1999). Application of a new optimization approach to the design of electrical wheels. *IEEE Transactions on Energy Conversion*, vol. 14, no. 4, (December 1999), pp.952-958, ISSN 0013-4457.

Gieras, J. F.; Wang, R.-J. & Kamper, M. J. (2004). *Axial Flux Permanent Magnet Brushless Machines*, Kluwer Academic Publishers, ISBN 978-1-4020-6993-2, Netherlands.

Helali H. et al. (2005). Power converter's optimisation and design. Discrete cost function with genetic based algorithms, *Proceedings of 11th Power Electronics and Applications Conference*, ISBN 91-7636-385-6, Dresden, Germany, September 2005.

Malyna, D. V.; Duarte, J. L.; Hendrix, M. A. M. & van Horck, F. B. M. (2007). Optimization of Combined Thermal and Electrical Behavior of Power Converters Using Multi-Objective Genetic Algorithms, *Proceedings of 12th Power Electronics and Applications Conference*, ISBN 0-7803-9457-7 Aalborg, Denmark, September 2007.

Miettinen, K. (1999), *Nonlinear Multiobjective Optimization*, Kluwer Academic Publishers, ISBN 978-0-7923-8278-2, Boston, USA.

Mohan, N.; Undeland, T. & Robbins, W. (2003), *Power Electronics: Converters, Applications and Design*, John Wiley & Sons, ISBN 978-0-471-22693-2, Hoboken, USA.

Nilssen, R.; Skaar, S. E.; Lund, R.; Skjellnes, T; Øvrebø, S. & Løvli E. (2005). Design of a permanent magnet synchronous integrated in the wheel rim on wheelchairs, *Proceedings of 11th Power Electronics and Applications Conference*, ISBN 91-7636-385-6, Dresden, Germany, September 2005.

Ocenasek, J. & Schwarz, J. (2002). Estimation distribution algorithm for mixed continuous-discrete optimization problems, *Proceedings 2nd Euro-International Symposium on Computational Intelligence*, ISBN 1-58603-256-9, Amsterdam, Nederland, September 2002.

Parviaien, A.; Niemelä, M. & Pyrhönen, J. (2003). Analytical, 2D FEM and 3D FEM Modeling of PM Axial Flux Machine, *Proceedings of 10th Power Electronics and Applications Conference*, ISBN 90-75815-06-9, Toulouse, France, September 2003.

Qu, R. & Lipo, T. A. (2002). Analysis and Modeling of Airgap & Zigzag Leakage Fluxes in a Surface-Mouted-PM Machine, *Proceedings of 37th Industry Applications Conference*, ISBN 0-7803-7420-7, Pittsburgh, USA, October 2002.

Sahin, F. & Vandenput, A. J. A. (1999). Design Considerations of the Flywheel-Mounted Axial-Flux Permanent Magnet Machine for a Hybrid Electric Vehicle, *Proceedings of 8th Power Electronics and Applications Conference*, ISBN 90-75815-06-9, Lausanne, Switzerland, September 1999.

Semikron (2010), "Application Manual", available from http://www.semikron.com/skcompub/en/application_manual-193.htm.

Skaar, S. E. & Nielssen, R. (2003). Genetic Optimization of Electric Machines, a State of the Art Study, *Proceedings of 10th Power Electronics and Applications Conference*, ISBN 90-75815-06-9, Toulouse, France, September 2003.

Socha, K. (2008). Ant colony optimization for continuous and mixed-variable domains, *PhD Thesis*, Université Libre de Bruxelles.

Tseng, K.-J. & Chen, G. H. (1997). Computer-Aided Design and Analysis of Direct-Driven Wheel Motor Drive. *IEEE Transactions on Power Electronics*, vol. 12, no. 3, (May 1997), pp. 517-527, ISSN 0885-8993.

Versèle, C. et al. (2009). Analytical Design of an Axial Flux Permanent Magnet In-Wheel Synchronous Motor for Electric Vehicle, *Proceedings of 13th Power Electronics and Application Conference*, ISBN 978-1-4244-1742-1, Barcelona, Spain, September 2009.

Versèle, C.; Deblecker, O. & Lobry, J. (2010). Multiobjective Optimal Design of Medium Frequency Transformers for Full-Bridge DC-DC Converters, *International Review of Electrical Engineering*, vol. 5, no. 4, (July-Augustus 2010), pp. 1354-1363, ISSN 1827-6660.

Yang, Y.-P.; Luh, Y.-P. & Cheung, C.-H. (2004). Design and Control of Axial-Flux Brushless DC Wheel Motors for Electric Vehicles – Part I: Multiobjective Optimal Design and Analysis. *IEEE Transactions on Magnetics*, vol. 40, no. 4, (July 2004), pp. 1873-1882, ISSN 0018-9464.

Yang, Y.-P. & Chuang, D.-S. (2007). Optimal Design and Control of a Wheel Motor for Electric Passengers Cars. *IEEE Transactions on Magnetics*, vol. 43, no. 1, (January 2007), pp. 51-61, ISSN 0018-9464.

Yu, P. L. (1973). A class of solutions for group decision problems, *Management Science*, vol. 19, no. 8, (April 1973), pp. 936-946, ISSN 0025-1909.

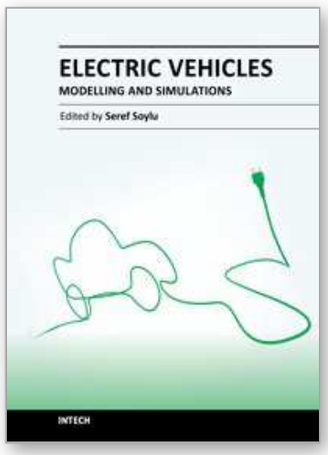

Electric Vehicles - Modelling and Simulations

Edited by Dr. Seref Soylu

ISBN 978-953-307-477-1
Hard cover, 466 pages
Publisher InTech
Published online 12, September, 2011
Published in print edition September, 2011

In this book, modeling and simulation of electric vehicles and their components have been emphasized chapter by chapter with valuable contribution of many researchers who work on both technical and regulatory sides of the field. Mathematical models for electrical vehicles and their components were introduced and merged together to make this book a guide for industry, academia and policy makers.

InTech Europe
University Campus STeP Ri
Slavka Krautzeka 83/A
51000 Rijeka, Croatia
Phone: +385 (51) 770 447
Fax: +385 (51) 686 166
www.intechopen.com

InTech China
Unit 405, Office Block, Hotel Equatorial Shanghai
No.65, Yan An Road (West), Shanghai, 200040, China
中国上海市延安西路65号上海国际贵都大饭店办公楼405单元
Phone: +86-21-62489820
Fax: +86-21-62489821

IntechOpen